

Article

# Lidar Studies of Wind Turbulence in the Stable Atmospheric Boundary Layer

Viktor A. Banakh \* and Igor N. Smalikho

V.E. Zuev Institute of Atmospheric Optics SB RAS, Tomsk 634055, Russia; smalikho@iao.ru

\* Correspondence: banakh@iao.ru; Tel.: +7-(3822)-49-29-65

Received: 4 July 2018; Accepted: 31 July 2018; Published: 3 August 2018



**Abstract:** The kinetic energy of turbulence, the dissipation rate of turbulent energy, and the integral scale of turbulence in the stable atmospheric boundary layer at the location heights of low-level jets (LLJs) have been measured with a coherent Doppler light detection and ranging (lidar) system. The turbulence is shown to be weak in the central part of LLJs. The kinetic energy of turbulence at the maximum velocity heights of the jet does not exceed  $0.1 \text{ (m/s)}^2$ , while the dissipation rate is about  $10^{-5} \text{ m}^2/\text{s}^3$ . On average, the integral scale of turbulence in the central part of the jet is about 100 m, which is two to three times less than the effective vertical size of the LLJ.

**Keywords:** coherent Doppler lidar; wind turbulence; stable boundary layer; low-level jet; turbulence energy; dissipation rate; integral scale

## 1. Introduction

Understanding the processes of turbulence in stably stratified flows remains a challenge in geophysical sciences. Stable atmospheric stratification usually occurs when the underlying surface is cooled in comparison to the surrounding environment. In the summer, this happens at night over land surfaces, or even during the day over large cold water areas. The formation of low-level jets (LLJs) at the height of the boundary layer is characteristic of stable stratification in the atmosphere. For an experimental study of the atmospheric boundary layer, both wind sensors installed at weather towers (see, for example, Ref. [1]) and remote sensing by sonic detection and ranging systems (sodars) and light detection and ranging systems (lidars) are used.

Experimental studies of LLJs with sodars have been the subject of, in particular, Refs. [2–5], which report the data on the frequency of LLJ occurrence and the distribution of heights of the axis and maximum velocities of the jets. Peculiarities were revealed in the variations of the standard deviation of the horizontal component of the wind velocity vector with the height at different velocities at the jet axis.

The results of lidar investigations of LLJs were published in Refs. [6–10]. In these papers, the data measured by the 2- $\mu\text{m}$  pulsed coherent Doppler lidar (PCDL) [11] are used to retrieve the vertical profiles of the mean wind and variance of the longitudinal component of the wind velocity vector  $\sigma_V^2$ . To obtain vertical profiles of the variance of wind velocity, the scanning by the probing beam in the vertical plane along the wind direction was used. The results of lidar [6–10] and sodar [2–5] studies of LLJs and wind velocity fluctuations in the stable atmospheric boundary layer (ABL) are in agreement in many aspects, and supplement each other. However, such parameters as the turbulent energy dissipation rate  $\varepsilon$  and the integral (outer) scale of turbulence  $L_V$  were not studied experimentally at the heights of LLJ till now.

It was shown [12,13] that the raw data measured by PCDL with the vertical scanning by the probing beam can be used not only to estimate the variance of wind velocity fluctuations as in

Refs. [6–10], but also to retrieve the vertical profiles of  $\varepsilon$  and  $L_V$ . However, this method gives a large error in the cases when narrow LLJ or strong horizontal wind shears arise [14].

A method for the estimation of the kinetic energy of turbulence  $E$ , dissipation rate  $\varepsilon$ , and the integral scale  $L_V$  from PCDL data at the conical scanning by the probing beam around the vertical axis was proposed in Ref. [15]. The method was tested in experiments with the Halo Photonics StreamLine Doppler wind lidar, and the results were obtained for the layer of intense turbulent mixing at the neutral and unstable thermal stratification in the atmosphere. These results were in agreement with the theory and available experimental data. In this paper, this method with some modification is applied to study of wind turbulence in the stable atmospheric boundary layer in the presence of LLJ. The results of lidar experiments at the territory of the Basic Experimental Observatory (BEO) of the Institute of Atmospheric Optics of the Siberian Branch of the Russian Academy of Sciences (SB RAS) in Tomsk and at the coast of Lake Baikal are analyzed.

## 2. Method for Determination of Turbulence Parameters

The method proposed in Ref. [15] consists essentially in the following. The probing beam of the pulsed coherent Doppler lidar rotates around the vertical axis with the constant angular velocity  $\omega_s$  at the fixed elevation angle, i.e., the angle between the beam optical axis and the horizontal plane at the lidar location height,  $\varphi$  [16]. From the raw lidar data after pre-processing, we obtain an array of estimates of the radial velocity (projection of the wind velocity vector on the probing beam axis)  $V_L(R_k, \theta_m; n)$  for different distances from the lidar to the center of the probing volume  $R_k$  and azimuth angles of scanning  $\theta_m$ . Distances from the lidar  $R_k$  and azimuth angles  $\theta_m$  are determined, correspondingly, by the relations  $R_k = R_0 + k\Delta R$  and  $\theta_m = m\Delta\theta$ , where  $k = 0, 1, 2, \dots, K - 1$ ;  $\Delta R$  is the range gate length;  $R_0$  is the distance to the first usable range gate;  $m = 0, 1, 2, \dots, M - 1$ ;  $\Delta\theta = \omega_s\Delta t$  is the azimuth angle resolution;  $\Delta t = N_a/f_p$  is the duration of the measurement of raw data that is used to obtain an estimate of the radial velocity at fixed  $R_k, \theta_m$ , and  $n$ ;  $N_a$  is the number of probing pulses used for data accumulation;  $f_p$  is the pulse repetition frequency;  $M = 2\pi/\Delta\theta$  ( $\Delta\theta$  in radians) is the number of rays for one complete scan at the azimuth angle ranging from 0 to 360°; and  $n = 1, 2, 3, 4, \dots$  is the scan number. The duration of one scan is  $T_{\text{scan}} = M\Delta t$ .

Along with the array of estimates of the radial velocity  $V_L(R_k, \theta_m; n)$ , the array of estimates of the signal-to-noise ratio  $\text{SNR}(R_k, \theta_m; n)$  is calculated from the same raw lidar data. The signal-to-noise ratio is defined as the ratio of the mean power of the lidar echo signal to the mean power of noise in the receiver passband of 50 MHz. The information about the signal-to-noise ratio can be used for determination of the maximum probing range (distance  $R_{K-1}$ ). The distances  $R_k$  correspond to the heights  $h_k = R_k \sin \varphi$ .

On the assumption that the wind is stationary (within one hour) and statistically homogeneous on the horizontal plane, from the array  $V_L(R_k, \theta_m; n)$ , we can estimate the vector of the mean wind velocity  $\langle \mathbf{V}(h_k) \rangle = \{ \langle V_z \rangle, \langle V_x \rangle, \langle V_y \rangle \}$ , where  $V_z$  is the vertical velocity component,  $V_x$  and  $V_y$  are the horizontal components, and the angular brackets denote an ensemble averaging. The sine-wave fitting [14] is used for estimation of  $\langle \mathbf{V}(h_k) \rangle$ . Then, fluctuations of lidar estimates of the radial velocities are calculated as:

$$V'_L(R_k, \theta_m; n) = V_L(R_k, \theta_m; n) - \mathbf{S}(\theta_m) \langle \mathbf{V}(h_k) \rangle \quad (1)$$

where  $\mathbf{S}(\theta_m) = \{ \sin \varphi, \cos \varphi \cos \theta_m, \cos \varphi \sin \theta_m \}$  is the unit vector along the optical axis of the probing beam. Then, the array of random components of the lidar estimate of radial velocity calculated by Equation (1) for every height  $h_k$  is used to estimate the averaged over all of the azimuth angles  $\theta_m$ , variance  $\bar{\sigma}_L^2$ , and azimuth structure function  $\bar{D}_L(\psi_l)$  of the radial velocity by the following equations:

$$\bar{\sigma}_L^2 = \frac{1}{N} \sum_{n=1}^N \frac{1}{M} \sum_{m=0}^{M-1} [V'_L(R_k, \theta_m; n)]^2 \quad (2)$$

$$\overline{D}_L(\psi_l) = \frac{1}{N} \sum_{n=1}^N \frac{1}{M-l} \sum_{m=0}^{M-l-1} [V'_L(R_k, \theta_m + \psi_l; n) - V'_L(R_k, \theta_m; n)]^2 \quad (3)$$

where  $N$  is the number of scans used for the ensemble averaging,  $\psi_l = l\Delta\theta$ , and  $l = 1, 2, 3, 4, \dots$ . In Equation (1), the value  $\langle \mathbf{V}(h_k) \rangle = \frac{1}{N} \sum_{n=1}^N \mathbf{V}(h_k; n)$  averaged over the number of scans can be used as an estimate of the vector  $\langle \mathbf{V}(h_k) \rangle$ . Here,  $\mathbf{V}(h_k; n)$  is an estimate of the velocity vector obtained by the sine-wave fitting of lidar estimates of the radial velocity at the  $n$ -th scan.

Within the inertial interval of turbulence  $\psi_l = l\Delta\theta < L_V$  ( $\Delta\theta$  in radians) [17], the turbulence energy dissipation rate  $\varepsilon$  is determined from the azimuth structure function  $\overline{D}_L(\psi_l)$  by the equation [15]:

$$\varepsilon = \left[ \frac{\overline{D}_L(\psi_l) - \overline{D}_L(\psi_1)}{A(l\Delta y_k) - A(\Delta y_k)} \right]^{\frac{3}{2}} \quad (4)$$

where the function  $A(l\Delta y_k) = 2 \int_0^\infty d\kappa_1 \int_0^\infty d\kappa_2 \Phi(\kappa_1, \kappa_2) H_{\parallel}(\kappa_1) H_{\perp}(\kappa_2) [1 - \cos(2\pi l \Delta y_k \kappa_2)]$  [15] is calculated theoretically for the Kolmogorov model of the two-dimensional (2D) turbulence spectrum,  $\Phi(\kappa_1, \kappa_2) = 0.0652(\kappa_1^2 + \kappa_2^2)^{-4/3} [1 + (8/3)\kappa_2^2 / (\kappa_1^2 + \kappa_2^2)]$ ,  $H_{\parallel}(\kappa_1) = [\exp\{- (\pi \Delta p \kappa_1)^2\} \sin c(\pi \Delta R \kappa_1)]^2$ ;  $H_{\perp}(\kappa_2) = [\sin c(\pi \Delta y_k \kappa_2)]^2$ ,  $\Delta p = c\sigma_p/2$ ;  $c$  is the speed of light;  $2\sigma_p$  is the probing pulse duration determined by the  $e^{-1}$  power level to the right and to the left of the peak point,  $\sin c(x) = \sin x/x$ ;  $A(\Delta y_k) = A(l\Delta y_k)$  at  $l = 1$ ; and  $\Delta y_k = \Delta\theta R_k \cos \varphi$  is the transverse dimension of the probed volume,  $l\Delta y_k < L_V$ . To meet the requirement  $l\Delta y_k < L_V$ , when planning the lidar experiment, we use the known data about typical values of the integral scale  $L_V$  under different atmospheric conditions and their variation with height [1,18,19].

The variance of the radial velocity  $\overline{\sigma}_r^2$  averaged over all of the azimuth angles  $\theta_m$  is determined as [15]:

$$\overline{\sigma}_r^2 = \overline{\sigma}_L^2 - \overline{D}_L(\psi_1)/2 + \varepsilon^{2/3} [F(\Delta y_k) + A(\Delta y_k)/2] \quad (5)$$

where  $F(\Delta y_k) = \int_0^\infty d\kappa_1 \int_0^\infty d\kappa_2 \Phi(\kappa_1, \kappa_2) [1 - H_{\parallel}(\kappa_1) H_{\perp}(\kappa_2)]$ . In contrast to the approaches used earlier [6–10], Equation (5) takes into account the averaging of the radial velocity over the probed volume. If the elevation angle is  $\varphi = \arctg(1/\sqrt{2}) \approx 35.3^\circ$ , then from the lidar estimate of the variance of radial velocity by Equation (5), we can find the kinetic energy of turbulence  $E$  as [15,20]:

$$E = (3/2)\overline{\sigma}_r^2 \quad (6)$$

On the assumption that the spatial structure of wind turbulence is described by the Karman model [21], for an estimation of the integral scale  $L_V$ , we can use the following equations [22]:

$$L_V = 0.6973 \overline{\sigma}_r^3 / \varepsilon \quad (7)$$

or, at  $\varphi = 35.3^\circ$  [15]:

$$L_V = 0.3796 E^{\frac{3}{2}} / \varepsilon \quad (8)$$

Within the inertial range, turbulence is locally isotropic; its structure obeys the 2/3 Kolmogorov–Obukhov law, and the structure function of the radial velocity within the inertial subrange depends only on the dissipation rate  $\varepsilon$  [17]. The variance of fluctuations of the wind velocity is determined by the turbulent inhomogeneities of all of the scales, and consequently, can be influenced by the anisotropy of turbulence. In case of turbulence anisotropy, the variance of the radial velocity  $\sigma_r^2 = \langle V_r^2 \rangle - \langle V_r \rangle^2$  is dependent on both the elevation angle  $\varphi$  and the azimuth angle  $\theta_m$ . The variance of the radial velocity  $\overline{\sigma}_r^2$  averaged over all of the azimuth angles  $\theta_m$  depends on the elevation angle  $\varphi$  only. The estimate  $L_V$  obtained by Equations (7) and (8) is the integral scale of turbulence averaged over all of the azimuth angles  $\theta_m$ . The estimate  $L_V$  by Equation (8) relates to  $\varphi = 35.3^\circ$ . However, the estimate  $L_V$  by Equation (7) is dependent on the angle  $\varphi$  because of  $\overline{\sigma}_r^2$ .

If regular variations of the wind velocity due to its nonstationarity and statistical inhomogeneity on the horizontal plane are comparable with or exceeding the turbulent fluctuations of the wind, then Equation (1) is inapplicable. In this case, to determine the fluctuating component of lidar estimates of the radial velocity, the high-frequency spatiotemporal filtering of lidar data is required. At the rather large number  $N$  (for example,  $N$  being no smaller than 30), we first find deviations of the estimates of radial velocity from the result of sine-wave fitting:

$$V_L''(R_k, \theta_m; n) = V_L(R_k, \theta_m; n) - \mathbf{S}(\theta_m)\mathbf{V}(h_k; n) \quad (9)$$

for each  $n$ -th scan. Then, the fluctuating components of lidar estimates of the radial velocity are calculated as:

$$V_L'(R_k, \theta_m; n) = V_L''(R_k, \theta_m; n) - \tilde{V}_L(R_k, \theta_m) \quad (10)$$

where:

$$\tilde{V}_L(R_k, \theta_m) = \frac{1}{N} \sum_{n=1}^N V_L''(R_k, \theta_m; n) \quad (11)$$

are averaged deviations of estimates of the radial velocity from the results of sine-wave fitting, which could differ significantly from zero in the case of statistical inhomogeneity of the wind in the horizontal plane. This approach is applicable if the length of the scanning circle  $L_k = 2\pi R_k \cos \varphi$  describing the trajectory of the center of the probed volume at the distance  $R_k$  from the lidar exceeds the integral scale of turbulence  $L_V$  by at least tenfold.

The accuracy of lidar estimates of the dissipation rate  $\varepsilon$ , the variance  $\overline{\sigma_r^2}$  (or the kinetic energy  $E$ ), and the integral scale  $L_V$  depends on the instrumental error of estimation of the radial velocity  $\sigma_e$  [14,15,23], which is the function of the signal-to-noise ratio (SNR), and the strength of wind turbulence. The error of estimation of turbulent parameters from lidar data was calculated from the data of closed numerical simulation of Doppler lidar operation in the turbulent atmosphere by the algorithm [22]. The experimental values of  $\sigma_e$ ,  $\varepsilon$ , and  $L_V$  were used as input parameters in this simulation. Based on the results of simulation, we have selected the data of measurements by the StreamLine lidar in Tomsk and on Lake Baikal with such a high SNR that they certainly provided the estimation of turbulence parameters in the stable boundary layer at the heights of LLJ location with acceptable error.

### 3. Results and Discussion

#### 3.1. Experiment at the Basic Experimental Observatory of the V.E. Zuev Institute of Atmospheric Optics SB RAS

The lidar experiment at the territory of Basic Experimental Observatory (latitude 56.475448°N, longitude 85.048115°E) of the V.E. Zuev Institute of Atmospheric Optics (IAO) SB RAS in Tomsk was carried out in July 2016. The continuous measurements by the StreamLine lidar with the conical scanning by the probing beam around the vertical axis at the elevation angle  $\varphi = 35.3^\circ$  were conducted from 19:00 Local Time (LT) on 20 July 2016 to 14:00 LT on 24 July 2016. The duration of one conical scan was  $T_{\text{scan}} = 1$  min, the time for accumulation of raw lidar data was  $\Delta t = 0.5$  s, the number of rays for one complete scan was  $M = 120$ , and the azimuth angle resolution was  $\Delta\theta = 3^\circ$ . To obtain estimates of wind turbulence parameters, we used the data measured by the lidar for  $N = 30$  scans (30 min). The range gate length  $\Delta R$  was set equal to 18 m, and the step in height was  $\Delta h = \Delta R \sin \varphi \approx 10$  m. For the more detailed description of the experiment, see Ref. [15].

Figure 1 shows the spatiotemporal distributions of the kinetic energy of turbulence, the dissipation rate of turbulent energy, and the integral scale of turbulence obtained for three days: July 21–23. One can clearly see the contrast between the turbulence intensity in daytime and night-time. At night, the turbulence is very weak due to the stability of thermal stratification. In the daytime, intense turbulent mixing occurs. The data for the turbulence kinetic energy and the dissipation rate calculated

by Equations (4)–(6) do not contradict the theory of the atmospheric boundary layer [18,19,24], and are in a good agreement with the results of measurements by the sonic anemometer [15]. The values of the integral scale of turbulence obtained with Equation (8) for the daytime, when the temperature stratification is neutral or unstable, are also in agreement with the known experimental data [1]. However, in the night-time under stable atmospheric conditions, obtained estimates of  $L_V$  have very large values, which certainly contradicts the theory. Areas of improbable estimates of  $L_V$  are colored in white in Figure 1d. Correspondingly, the correctness of quantitative estimates of  $E$  and  $\varepsilon$  in the night-time also raises doubts. It is worth stressing that during this experiment, the signal-to-noise ratio (SNR) was high enough in order that the error of estimation of turbulent parameters from lidar data was small, even for very weak turbulence.

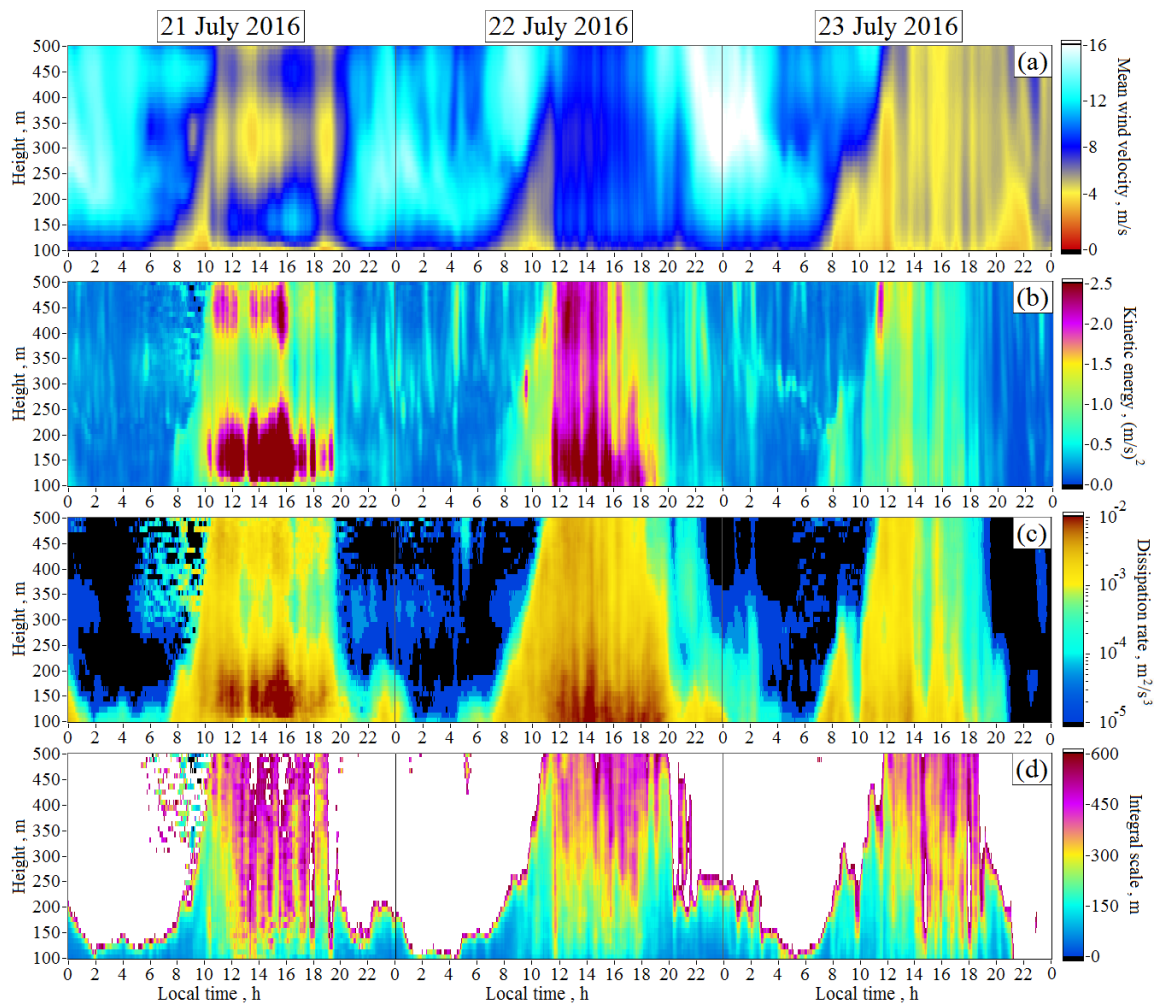


**Figure 1.** Spatiotemporal distributions of the mean velocity (a), kinetic energy of turbulence (b), dissipation rate of the kinetic energy of turbulence (c), and outer scale of turbulence (d) as obtained from the data of continuous measurements by the StreamLine lidar at the Basic Experimental Observatory of the Institute of Atmospheric Optics (IAO) SB RAS on 21–23 July 2016. In figures (c,d), estimates  $\varepsilon < 5 \times 10^{-5} \text{ m}^2/\text{s}^3$  are shown by the black color, and estimates  $L_V > 600 \text{ m}$  are shown by the white color.

Next, we consider the results of night-time lidar measurements in more detail. In the period of 20–24 July 2016, LLJ occurred three times: (1) from 22:00 on July 20 to 05:00 on July 21, (2) from 21:00 on July 21 to 06:00 on July 22, and (3) from 22:00 on July 22 to 04:00 on July 23 (hereinafter, local time is used). On the night of July 23–24, the jet stream was not observed. Figure 2 illustrates the

variation of the wind speed and direction with height. Each plot of this figure shows the vertical profiles retrieved from lidar measurements for one scan (1 min) every hour. Taking into account that these measurements were conducted at strongly stable temperature stratification, we can assume that variations of wind profiles for one hour are more likely caused by the nonstationary (mesoscale process) than by small-scale turbulence. Therefore, the application of the high-frequency time filtering by Equation (9) is quite justified.

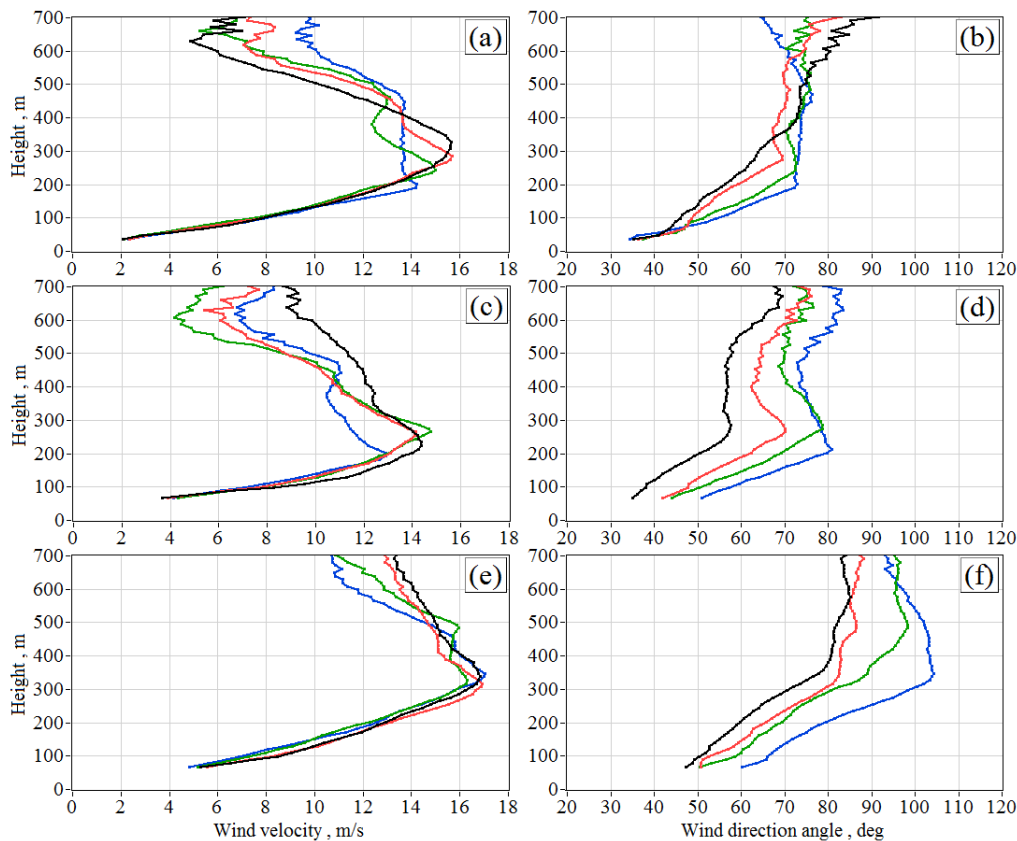


**Figure 2.** Vertical profiles of wind velocity (a,c,e) and wind direction angle (b,d,f) retrieved from measurements by the StreamLine lidar on 20–21 July (a,b), 21–22 July (c,d), and 22–23 July (e,f) of 2016 every hour at 23:00 (black curves), 00:00 (red curves), 01:00 (green curves), and 02:00 Local Time (LT) (blue curves). Each profile is obtained from one-minute measurements.

To reveal why the estimates of the turbulence parameters from night-time lidar data are incorrect, we have analyzed the spatially temporal inhomogeneity of the wind. Deviations of the radial velocity from the results of sine-wave fitting were calculated as functions of the azimuth angle and the distance between the lidar and the probed volume; that is, the distributions  $V_L''(R_k, \theta_m; n)$  were calculated by Equation (9). Figure 3 shows an example of the distributions  $V_L''(h_k / \sin \varphi, \theta_m; n)$  obtained from lidar measurements at four consecutive conical scans ( $n = 1, 2, 3, 4$ ) starting from 23:00 LT in the presence of LLJ with the maximum velocity at a height of about 350 m (see Figure 2e). It can be seen that for the layer adjacent to the ground up to a height of 250 m, the distributions  $V_L''(h_k / \sin \varphi, \theta_m; n)$  vary randomly from one scan to another. There are no doubts that these variations are caused by the turbulence. However, above this layer, random wind variations are transformed into a regular periodic structure, which remains practically unchanged during the lifetime of the LLJ, and disappears along with it.

Then, we consider the distribution averaged over time of measurement estimates of radial velocity fluctuations  $\tilde{V}_L(h_k / \sin \varphi, \theta_m)$  calculated by Equation (11) with  $N = 30$ . Figure 4 shows two examples of

these distributions. Figure 5 depicts the dependence  $\tilde{V}_L(h_k / \sin \varphi, \theta_m)$  on the azimuth angle at different heights obtained from lidar measurements on 23 July 2016 (the data are taken from Figure 4b).

It follows from the data shown in Figures 4 and 5 that temporal averaging smooths out random variations of  $V_L''(h_k, \theta_m; n)$ , but the regular deviations of lidar estimates of the radial velocity from the sine-wave fitting persist. The regular wind inhomogeneity leads to the overestimation of turbulent energy and the outer scale of turbulence, if Equation (1) is used to obtain the array of fluctuating components of lidar estimates of the radial velocity. To take into account the influence of the regular wind inhomogeneity, the wind turbulence parameters were estimated from the array of lidar estimates of radial velocity fluctuations corrected by Equation (10).

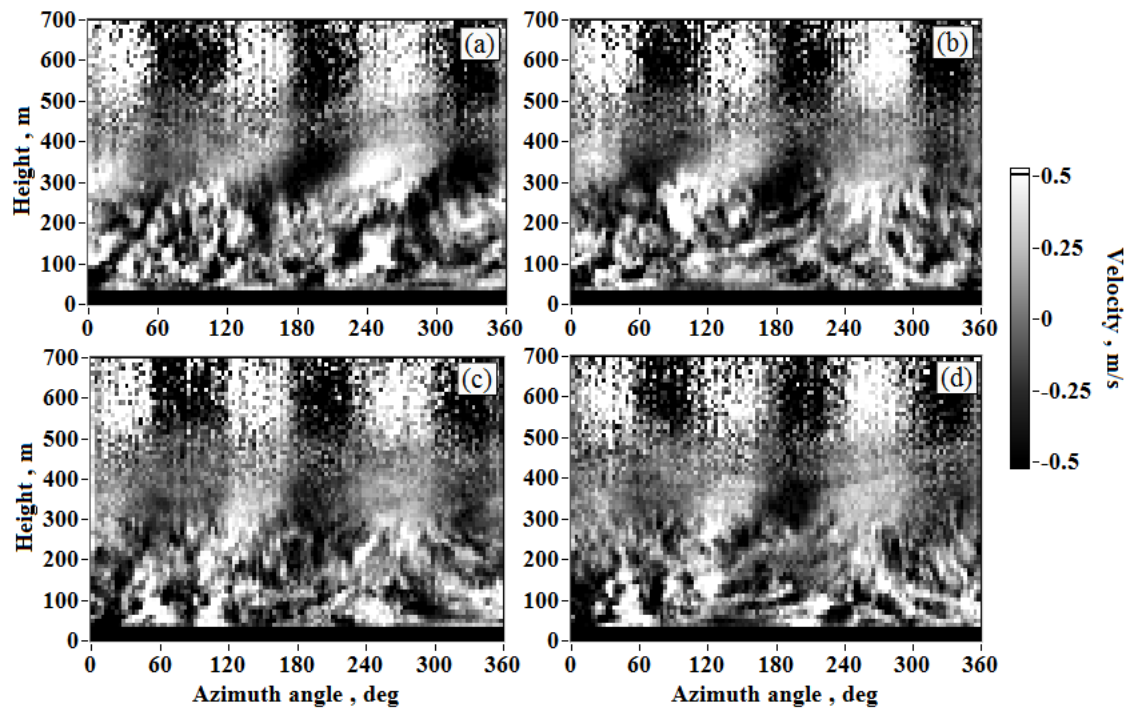


**Figure 3.** Distributions of estimates of radial velocity fluctuations  $V_L''(h_k / \sin \varphi, \theta_m; n)$  as obtained from measurements by the StreamLine lidar at 23:00 (a), 23:01 (b), 23:02 (c), and 23:03 (d) on 22 July 2016 with the use of Equation (9).

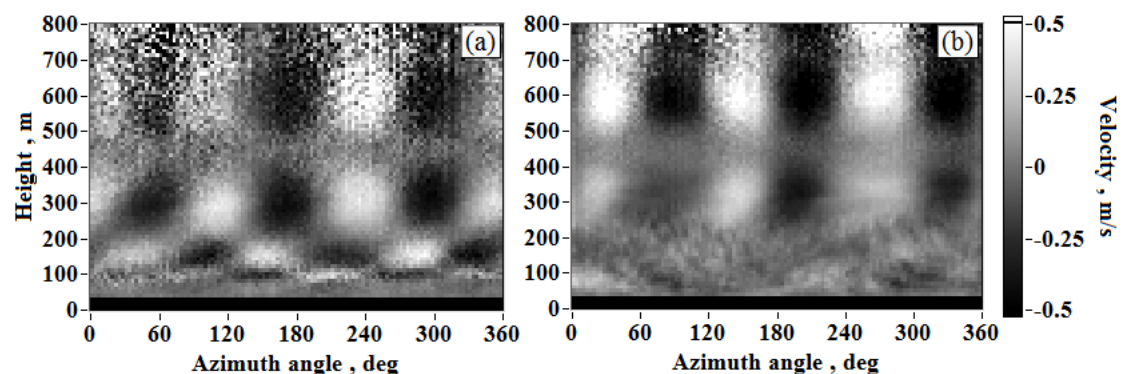


**Figure 4.** Distributions of averaged estimates of radial velocity fluctuations  $\tilde{V}_L(h_k / \sin \varphi, \theta_m)$  as obtained from measurements by the StreamLine lidar from 22:00 to 22:30 on 21 July 2016 (a) and from 00:00 to 00:30 on 23 July 2016 (b) with the use of Equation (11) at  $N = 30$ .

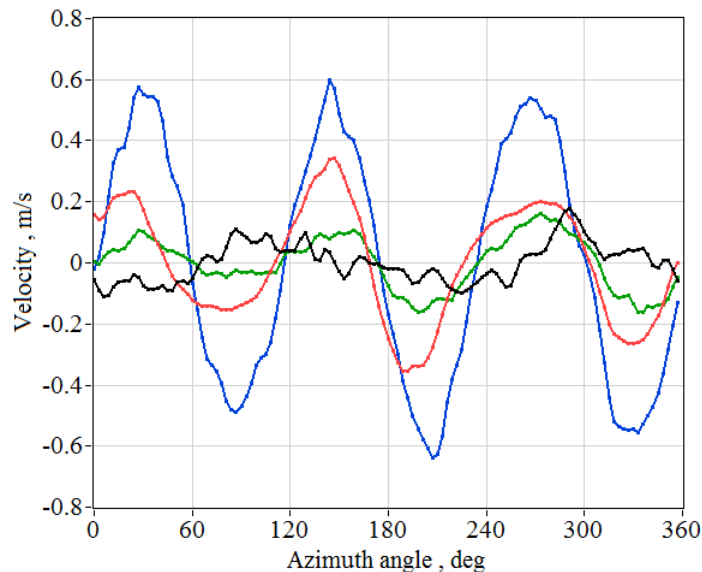


**Figure 5.** Dependence of  $\tilde{V}_L(h_k / \sin \varphi, \theta_m)$  on the azimuth angle  $\theta_m$  as obtained from measurements by the StreamLine lidar from 00:00 to 00:30 on 23 July 2016 at the heights  $h_k = 150$  m (black curve), 300 m (red curve), 450 m (green curve), and 600 m (blue curve).

By analogy with Ref. [15], we compared the azimuth structure functions of the radial velocity  $\overline{D}_a(\psi_l) = \overline{D}_L(\psi_l) - 2\sigma_\varepsilon^2$  obtained from experimental data with the use of Equation (10) with the structure functions calculated theoretically for the von Kármán model [21] for the two-dimensional spatial spectrum of wind velocity fluctuations:

$$D_\perp(l\Delta y_k) = \varepsilon^{2/3} A(l\Delta y_k; L_V) \tag{12}$$

where  $A(l\Delta y_k; L_V) = 2 \int_0^\infty d\kappa_1 \int_0^\infty d\kappa_2 \Phi(\kappa_1, \kappa_2; L_V) H_\parallel(\kappa_1) H_\perp(\kappa_2) [1 - \cos(2\pi l\Delta y_k \kappa_2)]$ , and  $\Phi(\kappa_1, \kappa_2; L_V)$  is described by Equation (27) from Ref. [15].

This comparison shows that we failed to completely remove the influence of the regular horizontal wind inhomogeneity. However, the value of the parameter:

$$\gamma = \left\{ L^{-1} \sum_{l=1}^L [\overline{D}_a(\psi_l) / D_\perp(l\Delta y_k) - 1]^2 \right\}^{1/2} \tag{13}$$

which was introduced in Ref. [15] and characterizes the degree of deviation of the experimental azimuth structure functions from the von Kármán model (12) becomes much less than the values of  $\gamma$  obtained without the high-frequency spatiotemporal filtering by Equations (9)–(11). On average,  $\gamma = 0.2$ , which is approximately twice as large as the average value of  $\gamma$  for the layer of intense turbulent mixing [15].

Figure 6 depicts the time dependence of lidar estimates of the wind turbulence parameters at heights in the vicinity of the maximal wind velocity in LLJ. It is seen from the figure that the use of Equations (9)–(11) in the calculation of fluctuations of the radial velocity measured by the lidar has allowed us to obtain estimates of the integral scale of turbulence under stable conditions in the atmosphere, which do not contradict the theory and the available experimental data [1,18,19]. The obtained results demonstrate that in the central part of LLJ, the integral scale of turbulence varies from 40 m to 150 m. On average, it is about 100 m. The kinetic energy of turbulence does not exceed  $0.03 \text{ (m/s)}^2$ , and the dissipation rate is less than  $3 \times 10^{-5} \text{ m}^2/\text{s}^3$  in the vicinity of the maximal jet stream velocity.

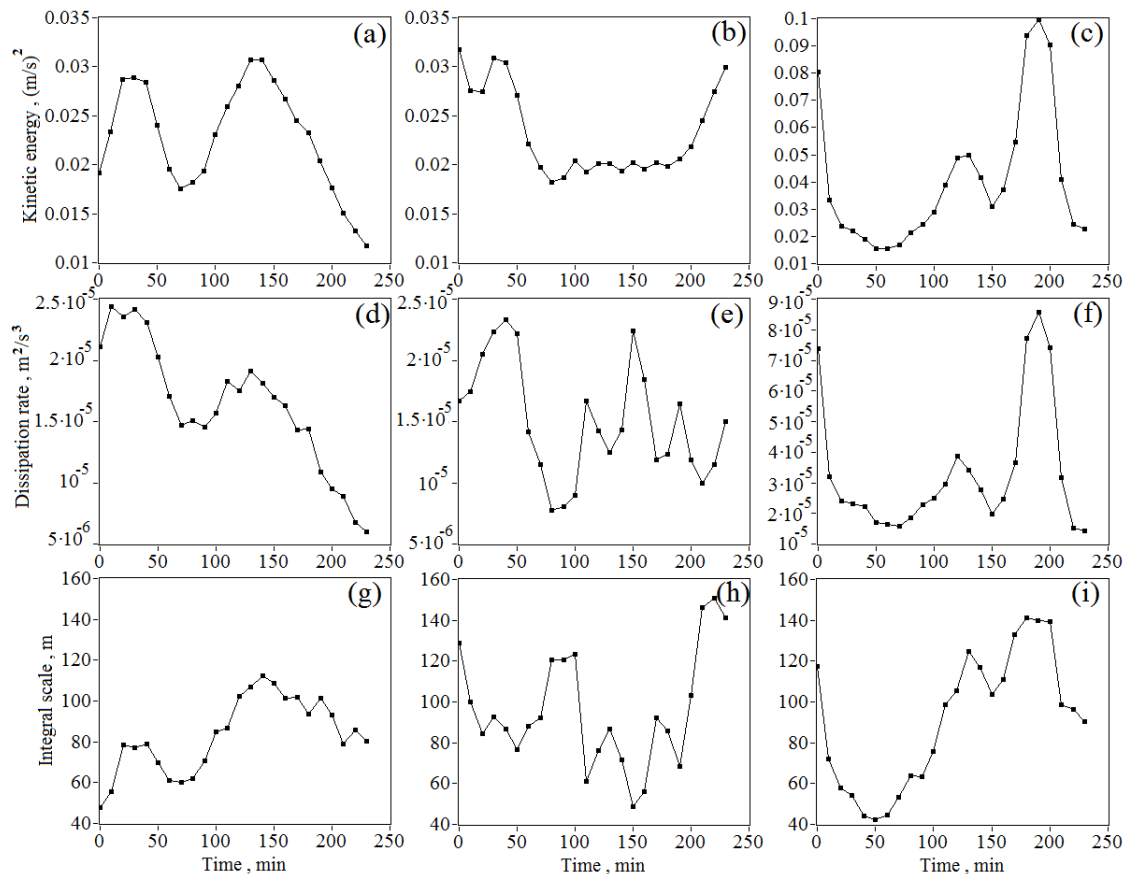


**Figure 6.** Temporal variations of the kinetic energy of turbulence (a–c), the dissipation rate (d–f), and the integral scale of turbulence (g–i) as obtained from measurements by the StreamLine lidar at 22:00 LT on 20 July 2016 (a,d,g), 22:00 LT on 21 July 2016 (b,e,h), and 22:30 LT on 22 July 2016 (c,f,i) at heights of 307 m (a,d,g), 254 m (b,f,h), and 317 m (c,f,i).

The results depicted in Figure 6 were obtained from measurements at a SNR from 0.1 to 0.3. At this SNR and the number of probing pulses used for accumulation of raw lidar data  $N_a = 7500$ , the instrumental error  $\sigma_e$  of estimation of the radial velocity by Equation (9) does not exceed 0.05 m/s [23]. At this instrumental error,  $M = 120$ , and  $N = 30$ , the condition:

$$[\overline{D}_L(\psi_i) - \overline{D}_L(\psi_1)] \gg \overline{D}_L(\psi_1) \sqrt{2/(MN)} \quad (14)$$

providing for the high accuracy of the estimation of the dissipation rate from lidar data [15,23] is fulfilled even at the very weak turbulence when  $\varepsilon$  does not exceed  $10^{-6} \text{ m}^2/\text{s}^3$ , and the variance  $\sigma_e^2$  is, on average, an order of magnitude less than the values of the kinetic energy of turbulence shown in Figure 6. According to our calculations, for the data in Figure 6, the relative errors of estimation of the turbulence energy and the dissipation rate vary from 5% to 7%, and those for the integral scale of turbulence range from 9% to 12%.

### 3.2. Experiment at the Lake Baikal Coast

The lidar experiment at the Lake Baikal Coast was carried out at the western coast near Listvyanka in August 2015. The StreamLine lidar was installed at the territory of the Baikal Astrophysical Observatory of the Institute of Solar-Terrestrial Physics SB RAS (latitude  $51.405230^\circ\text{N}$ , longitude  $104.673121^\circ\text{E}$ ) several tens of meters far from the Big Solar Vacuum Telescope (BSVT). The goal of the experiment was to study atmospheric internal waves (AIW) [16]. As at the Basic Experimental Observatory, the lidar measurements were conducted with the use of conical scanning by the probing

beam about the vertical axis. The following measurement parameters were set: elevation angle  $\varphi = 60^\circ$ ; angular scanning rate  $\omega_s = 10^\circ/\text{s}$ ; number of probing pulses for accumulation of raw data  $N_a = 3000$ ; step in the range  $\Delta R = 30\text{ m}$ . For the pulse repetition frequency of the StreamLine lidar,  $f_p = 15\text{ kHz}$ , the duration of data measurement for one ray was  $\Delta t = N_a/f_p = 0.2\text{ s}$ , the resolution in the azimuth angle was  $\Delta\theta = 2^\circ$ , the number of rays was  $M = 180$ , and the duration of one complete scan was  $T_{\text{scan}} = M\Delta t = 36\text{ s}$ .

The data of measurements from 01:00 to 08:00 LT of 24 August 2015 turned out to be the most suitable for the investigation of wind turbulence. In this period, the LLJ was observed, and the signal-to-noise ratio (SNR) of the lidar echo signal was large. After processing the raw data, we obtained two-dimensional height–time distributions of the signal-to-noise ratio, wind speed and direction, and the vertical component of the wind velocity vector. These distributions are shown in Figure 7. Each vertical profile was retrieved from measurements for one scan for 36 s. It is seen that the LLJ observed for 7 h was localized at heights of 450–750 m. At a height of about 300 m, the wind direction drastically changed to the opposite one: below this level, the wind was directed from the land, while above it, the wind was directed from the lake. At 07:00 LT, an internal wave occurred. It was observed for 30 min. This wave is clearly seen in Figure 7d for the vertical component of the wind velocity. The localization of the wave is shown by a black rectangle in Figure 7d. The period of this wave was approximately 6 min. The same wave motion is seen in the data for the average wind speed (Figure 7b) and direction (Figure 7c).

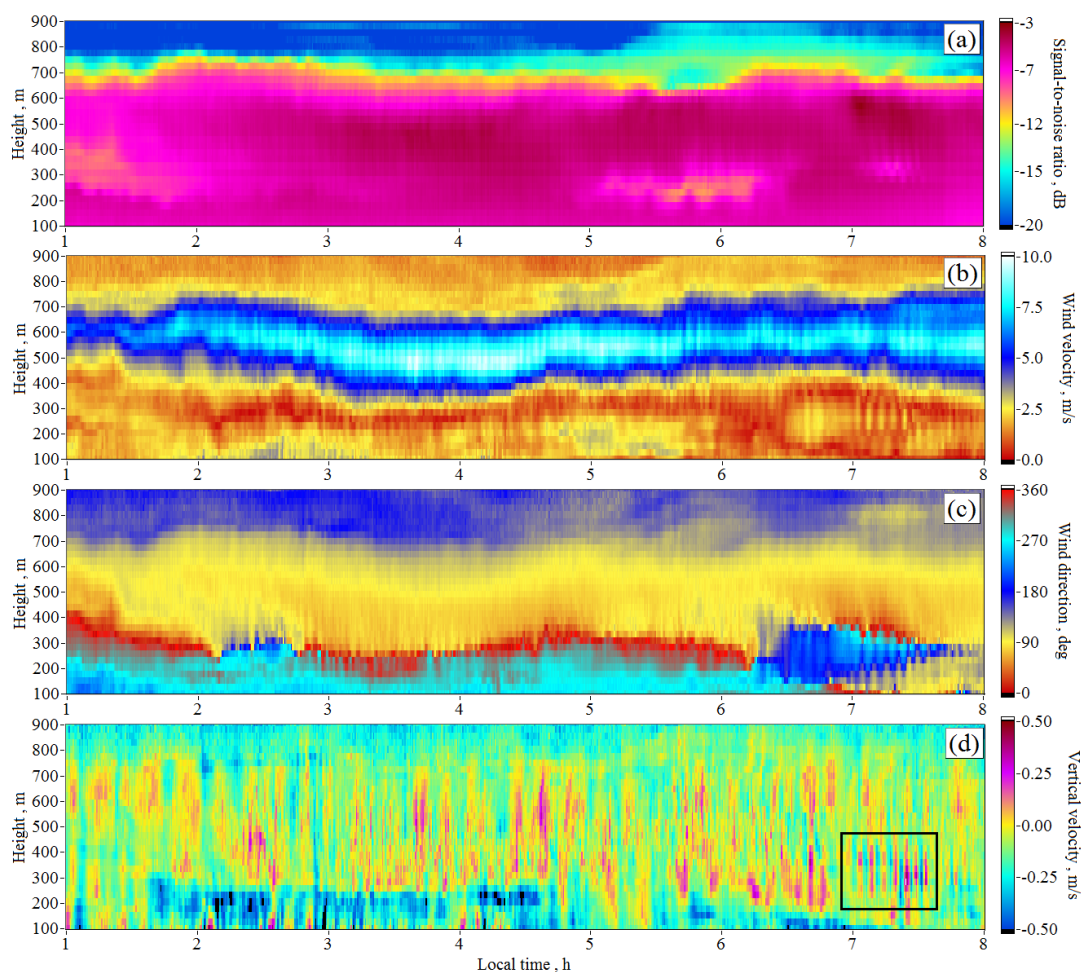


**Figure 7.** Heights and time distributions of the signal-to-noise ratio (SNR) (a), wind velocity (b), wind direction angle (c), and vertical component of the wind velocity vector (d), as obtained from measurements by the StreamLine lidar at the Lake Baikal coast on 24 August 2015.

In contrast to the lidar experiment at BEO (see the previous section), the analysis of the arrays of estimates of radial velocity fluctuations for the measurement period from 01:00 to 08:00 LT on 24 August 2015 did not reveal a regular inhomogeneity in the distributions  $V_L''(h_k/\sin\varphi, \theta_m; n)$ , even in the cases of extremely weak turbulence and AIW events. The analysis of the azimuth structure functions of radial velocity that was measured, in particular, at the heights of the central part of the jet stream has shown that these structure functions are well described by the von Kármán model, as in the experiment at BEO. This follows from the calculation of the parameter  $\gamma$  by Equation (13).

The dissipation rate of the turbulent energy  $\varepsilon$  can be determined from lidar data by Equation (4) only on the assumption of locally homogeneous and isotropic turbulence, and with the azimuth structure functions of radial velocity fluctuations measured within the inertial subrange of turbulent inhomogeneities [15]. Therefore, in determination of the dissipation rate, there are no strong restrictions to elevation angles  $\varphi$ . However, the kinetic energy of turbulence  $E = (\sigma_w^2 + \sigma_u^2 + \sigma_v^2)/2$  cannot be calculated from lidar measurements with the use of conical scanning at elevation angles different from  $35.3^\circ$  [15,20] because of the anisotropy of turbulence, due to which the variances of the wind vector components  $\sigma_w^2$ ,  $\sigma_u^2$ , and  $\sigma_v^2$  differ. For this reason, for the calculation of the integral scale of turbulence  $L_V$  from the Baikal lidar data, which were obtained under the scanning angle  $\varphi = 60^\circ$ , we used Equation (7) instead of Equation (8). The relative contribution of the vertical component of the wind velocity vector increased with the increase of the elevation angle, and the variance of the vertical velocity  $\sigma_w^2$  was always less than the variances of the horizontal components of the wind velocity  $(\sigma_u^2 + \sigma_v^2)/2$ . Thus, at  $\varphi = 60^\circ$ , the values of  $\bar{\sigma}_r^2$  and, consequently,  $L_V$  calculated by Equation (7) were underestimated in comparison with the estimates of these parameters obtained for the same heights from data measured under scanning angle  $\varphi = 35.3^\circ$ .

As in the experiments at BEO, to obtain single estimates of the turbulence parameters ( $\varepsilon$ ,  $\bar{\sigma}_r^2$ , and  $L_V$ ), we used the raw data measured by the lidar for 30 min. In this experiment, the duration of one scan was 36 s. Thus, 50 scans ( $N = 50$ ) were made for 30 min. The total number of estimates of the radial velocity in the array used for determination of the turbulence parameters was  $M \cdot N = 180 \times 50 = 9000$ .

Figure 8 depicts the spatiotemporal distributions of the wind turbulence parameters obtained from the Baikal measurements. These data have the time step  $T_{\text{scan}} = 36$  s and the height step  $\Delta h = \Delta R \sin\varphi = 26$  m. As an example, Figures 9 and 10 show the average wind velocity and the time profiles of the turbulence parameters (borrowed from Figure 8) at the fixed heights, and their vertical profiles at some instants. One can see that turbulence is weak in the layer of 100–200 m and in the top part of the LLJ at heights of 600–700 m. In these locations, the dissipation rate  $\varepsilon$  varied from  $10^{-6}$  to  $3 \times 10^{-4}$   $\text{m}^2/\text{s}^3$ , and the variance  $\bar{\sigma}_r^2$  ranged within 0.005–0.07  $(\text{m}/\text{s})^2$ . In the bottom part of the LLJ at heights of 300–500 m from 02:30 to 07:00 LT, the turbulence was much stronger, the dissipation rate took values in the range of  $5 \times 10^{-4}$  to  $2 \times 10^{-3}$   $\text{m}^2/\text{s}^3$ , and the variance changed from 0.1  $(\text{m}/\text{s})^2$  to 0.25  $(\text{m}/\text{s})^2$ . The temporal variations of the integral scale of turbulence  $L_V$  at the fixed heights in the layer of 300–500 m are not so large as the temporal variations of  $\varepsilon$  and  $\bar{\sigma}_r^2$  at these heights. On average, the integral scale in the layer of 300–500 m is approximately equal to 50 m. With height, the average integral scale increases from 30 m at a height of 100 m to 70–80 m at a height of 500 m, and varies from 80 m to 150 m in the central part of the LLJ at heights of 500–600 m. At the heights where the wind velocity is maximal, the integral scale of turbulence is about 100 m. The same average estimates of the integral scale ( $\sim 100$  m) for the central part of the jet stream at lower heights follow from the lidar measurements at BES at the scanning with the elevation angle  $\varphi = 35.3^\circ$ . That is, in the LLJ locations, the integral scale of turbulence is two to three times less than the vertical size of the jet.

The sharp increase of the integral scale  $L_V$  with heights in the layer of 600–700 m, as well as separate peaks of  $L_V$  at heights of 100–300 m, can be caused by errors in estimation of the turbulence parameters. Despite the rather high experimental signal-to-noise ratio (SNR) at which the instrumental error of estimate of the radial velocity  $\sigma_\varepsilon$  is very small, the value of  $\varepsilon$  may be significantly underestimated [15,23] because of the extremely low turbulence observed in the stable

atmosphere. As a consequence, the value of  $L_V$  calculated by Equation (7) becomes overestimated in the same proportion.

The relative errors of the estimates of the turbulence energy dissipation rate  $E_\epsilon$ , the variance of turbulent variations of the radial velocity  $E_\sigma$ , and the integral scale of turbulence  $E_L$  were calculated based on the closed numerical simulation of lidar measurement of the turbulence parameters by Equation [22]. The values of  $\sigma_\epsilon$ ,  $\epsilon$ ,  $\overline{\sigma_r^2}$ , and  $L_V$ , which are necessary for the calculation of the errors, were obtained from the raw lidar data of this experiment. In the experiment, the instrumental error  $\sigma_\epsilon$  did not exceed 0.12 m/s, at least up to a height of 600 m. At these values, with allowance made for the large number of the degrees of freedom  $M \cdot N = 9000$ , the instrumental error of estimation of the radial velocity exerts practically no influence on the accuracy of determination of the variance of wind velocity fluctuations  $\overline{\sigma_r^2}$  in Figure 8b. According to the calculations based on the simulation, the error  $E_\sigma$  is 6–7%.

The instrumental error  $\sigma_\epsilon$  more significantly affects the accuracy of estimation of the dissipation rate  $\epsilon$ , especially in the stable boundary layer when the turbulence is very weak. This occurs because the dissipation rate is calculated from the difference of the azimuth structure functions of the radial velocity within the inertial range of turbulence (4), and the number  $l$  taken as small as possible. It follows from the simulation that at heights of 100–600 m, the relative error of estimation of the dissipation rate  $E_\epsilon$  may exceed 20% in some cases. This worsens the accuracy of determination of the integral scale of turbulence. However, in the overwhelming majority of the cases, the error of estimation of the dissipation rate  $E_\epsilon$  is between 5–8%, and the relative error  $E_L$  varies within 10–13%.

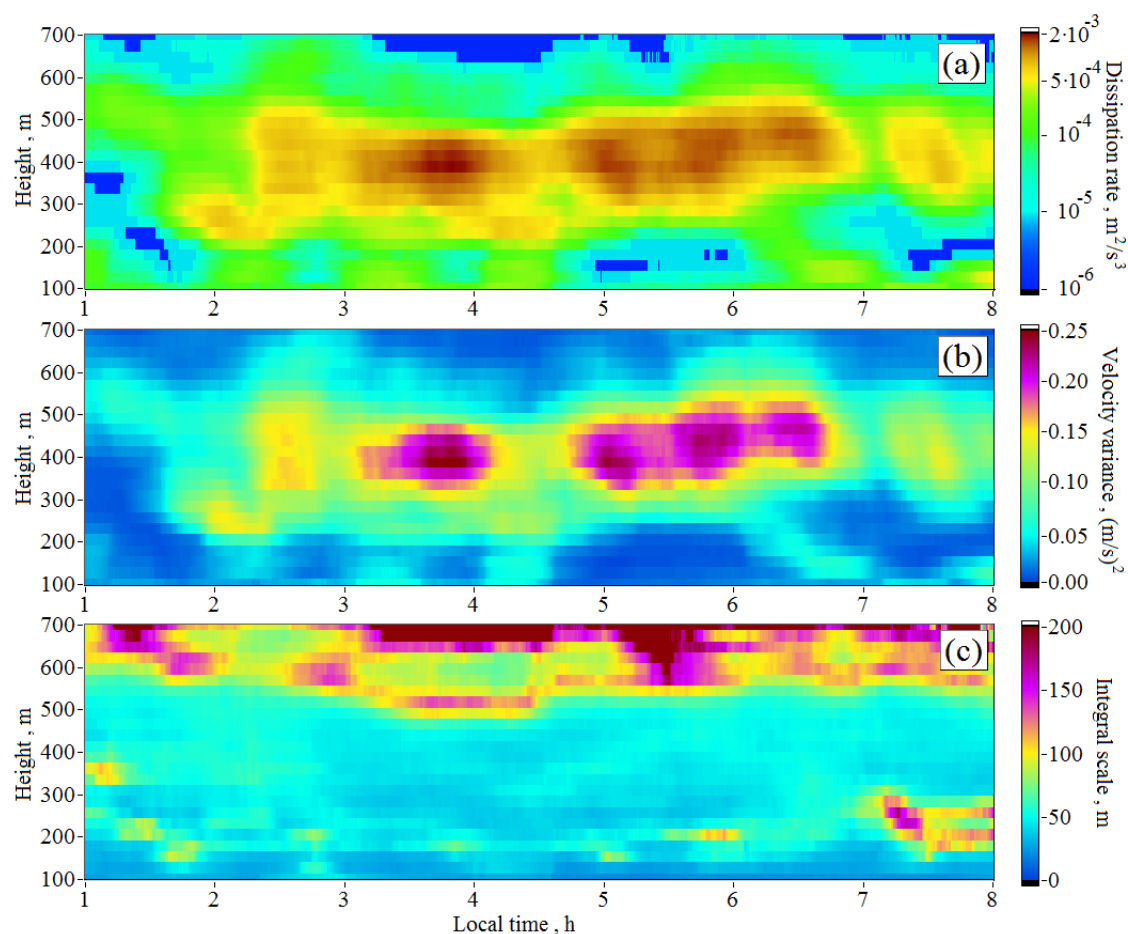


**Figure 8.** Height and time distributions of the turbulence energy dissipation rate (a), variance of turbulent fluctuations of the radial velocity (b), and the integral scale of turbulence (c) as obtained from measurements by the StreamLine lidar at the Lake Baikal coast on 24 August 2015.

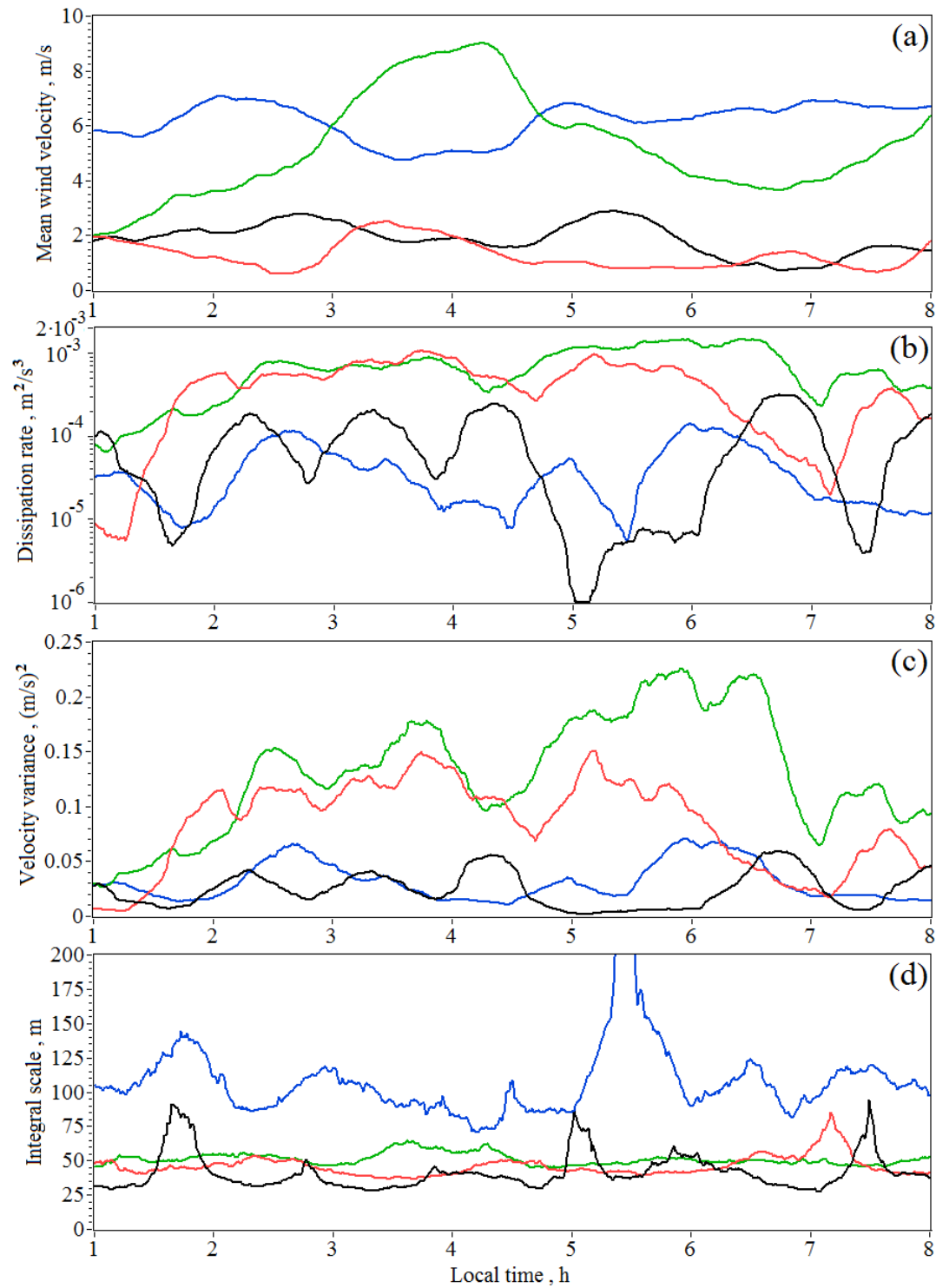


**Figure 9.** Temporal variations of the wind velocity (a), turbulence energy dissipation rate (b), variance of turbulent fluctuations of the radial velocity (c), and integral scale of turbulence (d) at heights of 150 m (black curves), 300 m (red curves), 450 m (green curves), and 600 m (blue curves), as obtained from measurements by the StreamLine lidar at the Baikal coast on 24 August 2015.

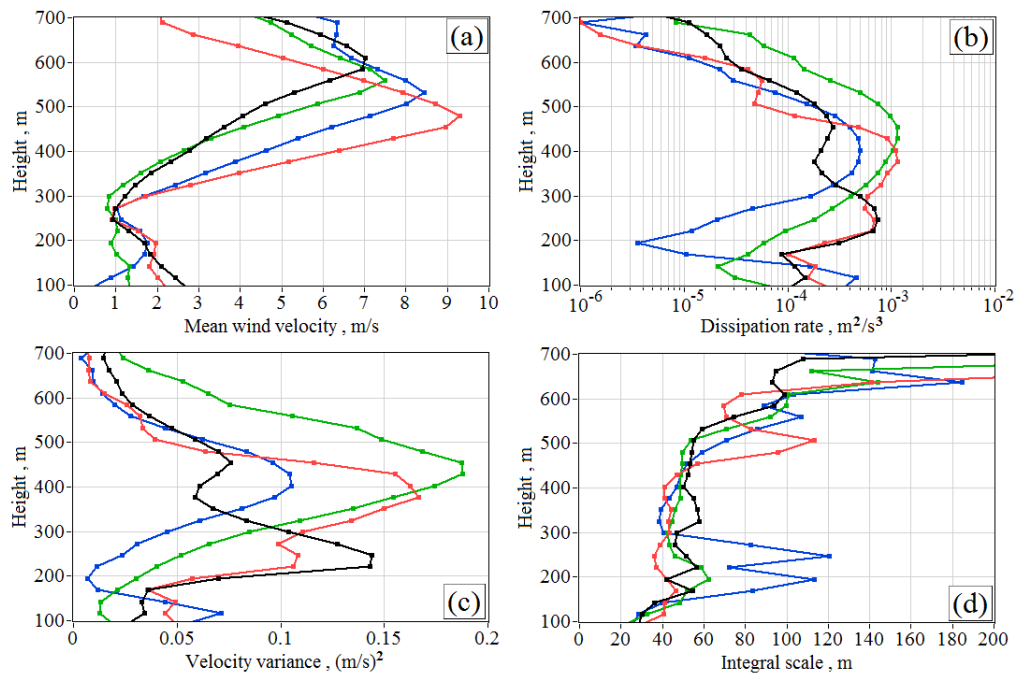


**Figure 10.** Vertical profiles of the mean wind velocity (a), turbulence energy dissipation rate (b), variance of turbulent fluctuations of the radial velocity (c), and integral scale of turbulence (d) retrieved from measurements by the StreamLine lidar at the Baikal coast on 02:00 (black curves), 04:00 (red curves), 06:00 (green curves), and 08:00 LT (blue curves) on 24 August 2015.

#### 4. Conclusions

Thus, this paper reports, for the first time, the results of lidar measurements of the dissipation rate of kinetic energy of turbulence and the integral scale of turbulence in the stable atmospheric boundary layer at the location heights of low-level jet streams. It has been found that during the LLJ lifetime, periodic regular inhomogeneity of the wind field in the horizontal direction can arise in the boundary layer. An origin of the regular horizontal inhomogeneity of the wind flow in the night-time boundary layer is unknown, and its study may be the subject of further investigations.

It has been found that the azimuth structure functions of the radial velocity measured by the lidar in stable low atmosphere at the heights of the central part of LLJ, as in the layer of intense turbulent mixing [15], are well described by the von Kármán model. It allows a method of azimuth structure function that was proposed in Ref.[15] for the estimation of the turbulent parameters from data of conically scanning PCDL in the layer of intense turbulent mixing, to use with some modification in stable atmospheric conditions. In all of the cases of observation of LLJs during the experiments in Tomsk and at the coast of Lake Baikal, the turbulence was weak in the central part of LLJ. Thus, the kinetic energy of turbulence at the heights of the maximum velocity at the center of LLJ does not exceed  $0.1 \text{ (m/s)}^2$ , and the dissipation rate is about  $10^{-5} \text{ m}^2/\text{s}^3$ . The dissipation rate of the turbulent energy in the bottom part of the LLJ can exceed that in the top part of jet by one to two orders of magnitude. In the central part of LLJ, the integral scale of turbulence is, on average, about 100 m, which is two to three times less than the effective vertical size of the jet.

**Author Contributions:** Conceptualization, V.A.B.; Methodology, V.A.B. and I.N.S.; Software, I.N.S.; Validation, V.A.B. and I.N.S.; Investigation, V.A.B. and I.N.S.; Writing-Original Draft Preparation, I.N.S.; Writing-Review & Editing, V.A.B.; Visualization, I.N.S.; Supervision, V.A.B.; Project Administration, V.A.B.; Funding Acquisition, V.A.B.

**Funding:** This research was funded by the Russian Science Foundation grant number 14-17-00386-II.

**Acknowledgments:** The authors are thankful to their colleagues from IAO SB RAS—A.V. Falits, A.A. Sukharev, and A.V. Galakhov for the help in the experiments.

**Conflicts of Interest:** The authors declare no conflict of interest. The funders had no role in the design of the study; in the collection, analyses, or interpretation of data; in the writing of the manuscript, and in the decision to publish the results.

## References

1. Byzova, N.L.; Ivanov, V.N.; Garger, E.K. *Turbulence in Atmospheric Boundary Layer*; Gidrometeoizdat: Leningrad, Russia, 1989; p. 265, ISBN 5-286-00151-3. (In Russian)
2. Kallistratova, M.A.; Kouznetsov, R.D.; Kuznetsov, D.D.; Kuznetsova, I.N.; Nakhaev, M.; Chirokova, G. The summertime low-level jet characteristics measured by sodars over rural and urban areas. *Meteorol. Z.* **2009**, *18*, 289–295. [[CrossRef](#)]
3. Kallistratova, M.A.; Kouznetsov, R.D. Low-level jets in the Moscow region in summer and winter observed with a sodar network. *Bound. Layer Meteorol.* **2012**, *143*, 159–175. [[CrossRef](#)]
4. Kallistratova, M.A.; Kouznetsov, R.D.; Kramar, V.F.; Kuznetsov, D.D. Profiles of wind speed variances within nocturnal low-level jets observed with a sodar. *J. Atmos. Ocean. Technol.* **2013**, *30*, 1970–1977. [[CrossRef](#)]
5. Prabha, T.V.; Leclerc, M.Y.; Karipot, A.; Hollinger, D.Y. Influence of nocturnal low-level jets on eddy-covariance fluxes over a tall forest canopy. *Bound. Layer Meteorol.* **2008**, *126*, 219–236. [[CrossRef](#)]
6. Newsom, R.K.; Banta, R.M. Shear-flow instability in the stable nocturnal boundary layer as observed by Doppler lidar during CASES-99. *J. Atmos. Sci.* **2003**, *60*, 16–33. [[CrossRef](#)]
7. Banta, R.M.; Newsom, R.K.; Lundquist, J.K.; Pichugina, Y.L.; Coulter, R.L.; Mahrt, L. Nocturnal low-level jet characteristics over Kansas during CASES-99. *Bound. Layer Meteorol.* **2002**, *105*, 221–252. [[CrossRef](#)]
8. Banta, R.M.; Pichugina, Y.L.; Newsom, R.K. Relationship between low-level jet properties and turbulence kinetic energy in the nocturnal stable boundary layer. *J. Atmos. Sci.* **2003**, *60*, 2549–2555. [[CrossRef](#)]
9. Banta, R.M.; Pichugina, Y.L.; Brewer, W.A. Turbulent velocity-variance profiles in the stable boundary layer generated by a nocturnal low-level jet. *J. Atmos. Sci.* **2006**, *63*, 2700–2719. [[CrossRef](#)]
10. Pichugina, Y.L.; Banta, R.M.; Kelley, N.D.; Brewer, W.A. Nocturnal boundary layer height estimate from Doppler lidar measurements. In Proceedings of the 18th Symposium on Boundary Layer and Turbulence, Stockholm, Sweden, 10 June 2008; Volume 7B.6.
11. Grund, C.J.; Banta, R.M.; George, J.L.; Howell, J.N.; Post, M.J.; Richter, R.A.; Weickman, A.M. High-resolution Doppler lidar for boundary layer and cloud research. *J. Atmos. Ocean. Technol.* **2001**, *18*, 376–393. [[CrossRef](#)]
12. Smalikho, I.; Köpp, F.; Rahm, S. Measurement of atmospheric turbulence by 2- $\mu\text{m}$  Doppler lidar. *J. Atmos. Ocean. Technol.* **2005**, *22*, 1733–1747. [[CrossRef](#)]
13. Banakh, V.A.; Smalikho, I.N.; Pichugina, E.L.; Brewer, W.A. Representativeness of Measurements of the Dissipation Rate of Turbulence Energy by Scanning Doppler Lidar. *Atmos. Ocean. Opt.* **2010**, *23*, 48–54. [[CrossRef](#)]
14. Banakh, V.A.; Smalikho, I.N. *Coherent Doppler Wind Lidars in a Turbulent Atmosphere*; Artech House: Boston, MA, USA; London, UK, 2013; p. 248, ISBN-13:978-1-60807-667-3.
15. Smalikho, I.N.; Banakh, V.A. Measurements of wind turbulence parameters by a conically scanning coherent Doppler lidar in the atmospheric boundary layer. *Atmos. Meas. Tech.* **2017**, *10*, 4191–4208. [[CrossRef](#)]
16. Banakh, V.A.; Smalikho, I.N. Lidar observations of atmospheric internal waves in the boundary layer of atmosphere on the coast of Lake Baikal. *Atmos. Meas. Tech.* **2016**, *9*, 5239–5248. [[CrossRef](#)]
17. Kolmogorov, A.N. Local structure of turbulence in incompressible viscous fluid at very large Reynolds numbers. *Doklady Akademii Nauk SSSR* **1941**, *30*, 299–303. [[CrossRef](#)]
18. Monin, A.S.; Yaglom, A.M. *Statistical Fluid Mechanics, Volume II: Mechanics of Turbulence*; M.I.T. Press: Cambridge, MA, USA, 1971; ISBN1-13 978-0486458915, ISBN2-10 0486458911.
19. Lumley, J.L.; Panofsky, H.A. *The Structure of Atmospheric Turbulence*; Interscience: New York, NY, USA, 1964.
20. Eberhard, W.L.; Cupp, R.E.; Healy, K.R. Doppler lidar measurement of profiles of turbulence and momentum flux. *J. Atmos. Ocean. Technol.* **1989**, *6*, 809–819. [[CrossRef](#)]
21. Von Kármán, T. Progress in the statistical theory of turbulence. *Proc. Natl. Acad. Sci. USA* **1948**, *34*, 530–539. [[CrossRef](#)] [[PubMed](#)]
22. Smalikho, I.N.; Banakh, V.A. Accuracy of Estimation of the Turbulent Energy Dissipation Rate from Wind Measurements with a Conically Scanning Pulsed Coherent Doppler Lidar. Part I. Algorithm of Data Processing. *Atmos. Ocean. Opt.* **2013**, *26*, 404–410. [[CrossRef](#)]

23. Banakh, V.A.; Smalikho, I.N.; Falits, A.V. Estimation of the turbulence energy dissipation rate in the atmospheric boundary layer from measurements of the radial wind velocity by micropulse coherent Doppler lidar. *Opt. Express* **2017**, *25*, 22679–22692. [[CrossRef](#)] [[PubMed](#)]
24. Zilitinkevich, S.S. *Dynamics of Atmospheric Boundary Layer*; Gidrometeoizdat: Leningrad, Russia, 1970; p. 292. (In Russian)



© 2018 by the authors. Licensee MDPI, Basel, Switzerland. This article is an open access article distributed under the terms and conditions of the Creative Commons Attribution (CC BY) license (<http://creativecommons.org/licenses/by/4.0/>).